

Time-dependent models of dense PDRs with complex molecules

Oscar Morata^{1*} and Eric Herbst²

¹ *Department of Physics, The Ohio State University, Columbus, OH 43210, USA*

² *Departments of Physics, Astronomy, and Chemistry, The Ohio State University, Columbus, OH 43210, USA*

29 October 2018

ABSTRACT

We present a study of the chemistry of a dense photon-dominated region (PDR) using a time-dependent chemical model. Our major interest is to study the spatial distribution of complex molecules such as hydrocarbons and cyanopolyynes in the cool dense material bordering regions where star formation has taken place. Our standard model uses a homogeneous cloud of density $2 \times 10^4 \text{ cm}^{-3}$ and temperature $T = 40 \text{ K}$, which is irradiated by a far-ultraviolet radiation field of intermediate intensity, given by $\chi = 100$. We find that over a range of times unsaturated hydrocarbons (e.g., C_2H , C_4H , C_3H_2) have relatively high fractional abundances in the more external layers of the PDR, whereas their abundances in the innermost layers are several orders of magnitudes lower. On the other hand, molecules that are typical of late-time chemistry are usually more abundant in the inner parts of the PDR. We also present results for models with different density, temperature, intensity of the radiation field and initial fractional abundances. Our results are compared with both high- and moderate-angular resolution observations of the Horsehead nebula. Our standard model is partially successful in reproducing the observations. Additional models run with different physical parameters are able to reproduce the abundance of many of the observed molecules, but we do not find a single model that fits all the observations at the same time. We discuss the suitability of a time-dependent model of a dense PDR such as ours as an estimator of the age of a PDR, provided that enough observational data exist.

Key words: ISM: molecules – ISM: abundances – Stars: formation – astrochemistry – molecular processes

1 INTRODUCTION

Far-ultraviolet (FUV) photons ($6 \text{ eV} < h\nu < 13.6 \text{ eV}$) can drastically affect the structure, chemistry, thermal balance, and evolution of portions of the interstellar medium, even if only the mean galactic interstellar radiation field (ISRF) is present. For this reason, the simplest chemical models of dense interstellar clouds should include a treatment of the radiative transfer of this radiation through the outer and intermediate layers of material, because the field affects observations that also sample the interior gas. Indeed, most of the molecular gas and certainly all the atomic gas of the Galaxy is found in regions where the FUV photon flux is several times that of the mean ISRF (Hollenbach & Tielens

1997). Photon-dominated regions (PDRs) are special regions of neutral gas exposed to intense fluxes of FUV radiation, which dominate the physical (heating) and chemical processes that take place in their interiors. PDRs can be observed in very different environments, including dense molecular clouds such as the Orion Bar or the Horsehead nebula, planetary nebulae, winds of red giants and AGB stars, the interstellar medium of starburst galaxies such as M82, low metallicity dwarf galaxies, etc. PDRs are studied through atomic spectral lines such as $[\text{C II}]$ at $158 \mu\text{m}$, $[\text{O I}]$ at 63 and $146 \mu\text{m}$, $[\text{C I}]$ at 370 and $609 \mu\text{m}$; many H_2O lines; millimetre and sub-millimetre rotational transitions of molecules such as CO , ^{13}CO , or C^{18}O ; ro-vibrational and pure rotational lines of H_2 ; and many broad mid-IR features attributed to PAHs.

Physical conditions of PDRs are thus very diverse. They can be diffuse, with gas density $n \sim 10 - 100 \text{ cm}^{-3}$, or dense, with $n > 10^4 \text{ cm}^{-3}$, while the incident FUV flux may

* Currently at the Institute of Astronomy and Astrophysics, Academia Sinica & Department of Earth Sciences, National Taiwan Normal University, 88, Sec. 4, Ting-Chou Road, Taipei 11677, Taiwan, ROC

Table 1. Standard initial (dark cloud) fractional abundances with respect to n_{H}

H ₂	0.5	C ₂ H	1.0×10^{-8}
H	7.5×10^{-5}	CO ₂	1.3×10^{-8}
He	0.14	H ₂ O	3.5×10^{-8}
C	2.8×10^{-8}	HCN	1.0×10^{-8}
O	1.0×10^{-4}	HNC	1.0×10^{-8}
N	1.3×10^{-5}	NH ₃	1.0×10^{-8}
S	7.2×10^{-8}	SO ₂	5.0×10^{-10}
Si	7.8×10^{-9}	C ₃ H	5.0×10^{-9}
Cl	4.0×10^{-9}	C ₄ H	4.5×10^{-8}
Fe	3.9×10^{-10}	C ₃ H ₂	5.0×10^{-9}
Mg	1.9×10^{-9}	HC ₃ N	1.0×10^{-8}
Na	4.7×10^{-10}	C ⁺	4.7×10^{-9}
P	3.0×10^{-9}	H ⁺	4.2×10^{-10}
CH	1.0×10^{-8}	He ⁺	3.5×10^{-10}
CN	2.5×10^{-9}	Fe ⁺	2.6×10^{-9}
CO	7.3×10^{-5}	Mg ⁺	5.1×10^{-9}
CS	2.0×10^{-9}	Na ⁺	1.5×10^{-9}
N ₂	4.2×10^{-6}	S ⁺	1.2×10^{-9}
NO	1.5×10^{-8}	Si ⁺	2.5×10^{-10}
O ₂	8.1×10^{-8}	H ₃ ⁺	1.4×10^{-9}
OH	1.0×10^{-7}	HCO ⁺	4.0×10^{-9}
S ₂	1.8×10^{-9}	HCS ⁺	2.0×10^{-10}
SO	1.0×10^{-9}	N ₂ H ⁺	2.0×10^{-10}

range from the ISRF to 10^6 times the ISRF very near to an O star. An important characteristic of PDRs is that they have a layered structure, as a result of the interaction of the radiation with the gas and dust. Typically, they contain an outer layer of partially ionised gas, where H is atomic and the predominant form of carbon is C II; a layer of neutral gas, where H₂ is predominant and carbon is present mainly as C I; and a molecular layer, where CO is the main form of carbon. The ratio between the flux of the incident radiation field and the gas density determines the size of these layers. The distinct layers should be observable if the PDR is seen edge-on, because then the geometry of the cloud is more apparent. One of the main difficulties of the study of PDRs is, however, the determination of the geometry of the object. The gas temperature is also dependent on the strength of the radiation field and the position inside the cloud, and can range from 10-100 K in the molecular layer to more than 10^3 K in the surface layers.

Dense PDRs are of particular interest in our attempt to understand the process of star formation. Newly formed stars produce high intensity photon fields deep inside clouds that lead to the formation of H II regions and, further removed from the exciting stars, PDRs. The gas-phase chemistry that occurs under these conditions is in most layers greatly different from the chemistry found in quiescent regions. The abundances of some atoms or molecules are greatly enhanced by the presence of the FUV field, while other species are destroyed by the radiation. For instance, the abundances of several hydrocarbons (C₂H, c-C₃H₂, C₄H, C₆H) have been found to be almost as high in relatively unshielded regions as in dark clouds (Fuente et al. 2003; Teyssier et al. 2004). However, some of these high abundances are difficult to explain with normal gas-phase chemi-

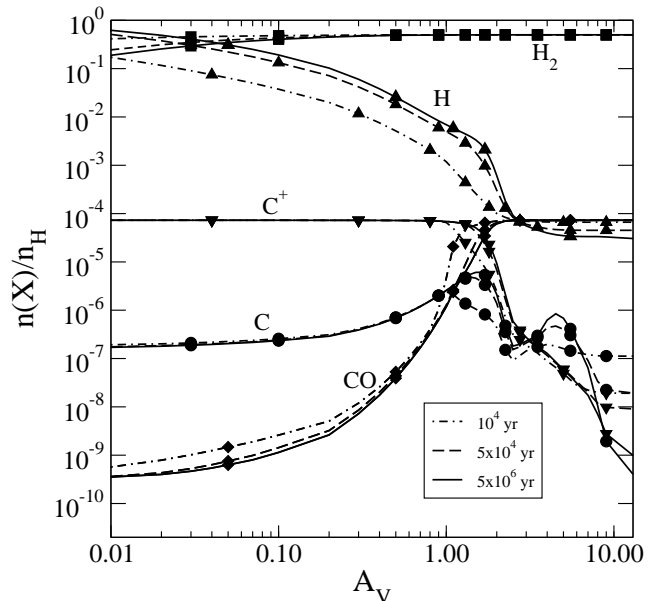


Figure 1. Fractional abundances of H (filled triangles), H₂ (filled squares), C (filled circles), C⁺ (filled triangles pointed downward), and CO (filled diamonds) with respect to n_{H} as a function of A_V for our standard model. Three different times are shown: 10^4 yr (dashed-dotted lines), 4×10^4 yr (dashed lines), and 5×10^6 yr (solid lines). The solid lines correspond to steady-state abundances.

cal models and a link between small hydrocarbons and PAHs has been proposed (Teyssier et al. 2004).

In this paper, we study the chemistry of a dense PDR created after a star has been formed inside a dark cloud. We are particularly interested in the spatial distributions of hydrocarbons and other complex molecules, and whether or not time-dependent chemistry can explain some of the discrepancies found between the observed abundances and the results of steady-state models (Teyssier et al. 2004; Pety et al. 2005) for the Horsehead nebula, as well as providing us with some estimate of the age of this PDR. Another use of time-dependent PDR chemistry is described by Bell et al. (2005). The structure of the remainder of the paper is as follows: in Section 2, we describe the time-dependent chemical model used. Our results obtained with our standard model are then considered in Section 3, while in Section 4 we discuss the dependence of our results on assorted physical parameters. The agreement between model results and observations of the Horsehead nebula is probed as a function of time in Section 5. Finally, Section 6 contains a summary of the paper.

2 MODEL

In our model, based on Lee et al. (1996), we assume a semi-infinite plane-parallel cloud divided into n_i slabs, on one side of which impinges an ultraviolet radiation field, defined in our case in units of the Draine (1978) standard radiation field scaled by a multiplicative factor χ . The visual extinction, A_V , and the total column density, N_{H} , are related by $A_V = 6.289 \times 10^{-22} N_{\text{H}}$ (Wagenblast & Hartquist 1989).

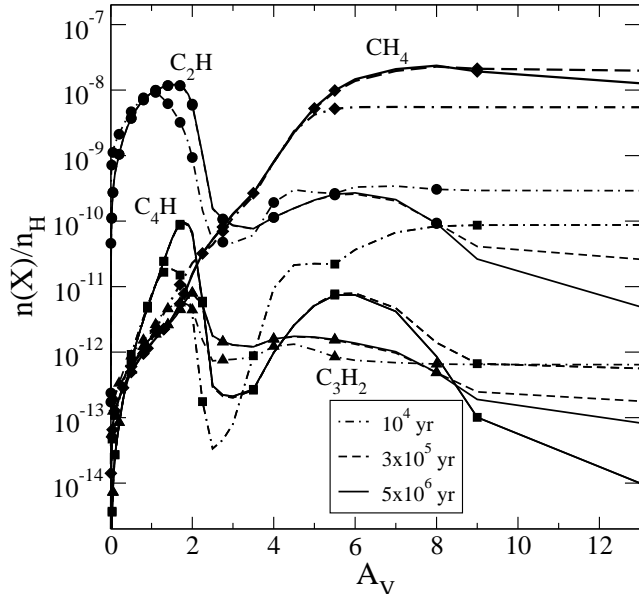


Figure 2. Fractional abundances of the molecules CH_4 (filled diamonds), C_2H (filled circles), C_4H (filled squares), and C_3H_2 (filled triangles) with respect to n_{H} as a function of A_V for our standard model. Three different times are shown: 10^4 yr (dashed-dotted line), 3×10^5 yr (dashed line), and 5×10^6 yr (solid line). The solid lines correspond to steady-state abundances.

The model treats radiative transfer and, in particular, takes into account the self- and cross-shielding due to H_2 and CO . We use the Draine & Bertoldi (1996) analytical approximation formula to calculate the H_2 photo-dissociation rate ($b = 1 \text{ km s}^{-1}$), which we have found to be in closer agreement with the results of the ‘exact’ treatment of H_2 self-shielding (Le Petit, Roueff & Le Boulbot 2002) than the method presented in Lee et al. (1996). However, the larger differences are only found for small values of the visual extinction, $A_V < 0.01$, which are not the main source of interest of the present paper. For the CO photodissociation rate, we use the same method as in Lee et al. (1996).

For our standard model, we have assumed a homogeneous cloud with physical conditions similar to those observed in the Horsehead nebula (see Section 5), namely a density $n_{\text{H}} = 2 \times 10^4 \text{ cm}^{-3}$ and a temperature $T = 40 \text{ K}$. The cosmic-ray ionisation rate, ζ , is assumed to be $1.3 \times 10^{-17} \text{ s}^{-1}$. We use a value for the scaling factor of the radiation field of $\chi = 100$, which is similar to the one measured in the Horsehead nebula (Zhou et al. 1993; Abergel et al. 2003). In our standard model, the cloud is divided into 42 slabs of differing length, defined in a way so as to have a smooth distribution of visual extinction points from $A_V = 5 \times 10^{-4}$ to $A_V = 13$, but good coverage of the positions where the fractional abundances of most of the species show steeper slopes. The time-dependent gas-phase chemistry is solved slab-wise, starting from the outermost slab and moving successively inward. The model solves a system of ordinary differential equations with the Gear method for each slab using the H_2 and CO photodissociation rates from the $(i-1)$ th slab as the input values for the i -th slab. For the chemistry, we use the `osu.2003` (Smith, Herbst & Chang 2004) gas-phase chemical network,

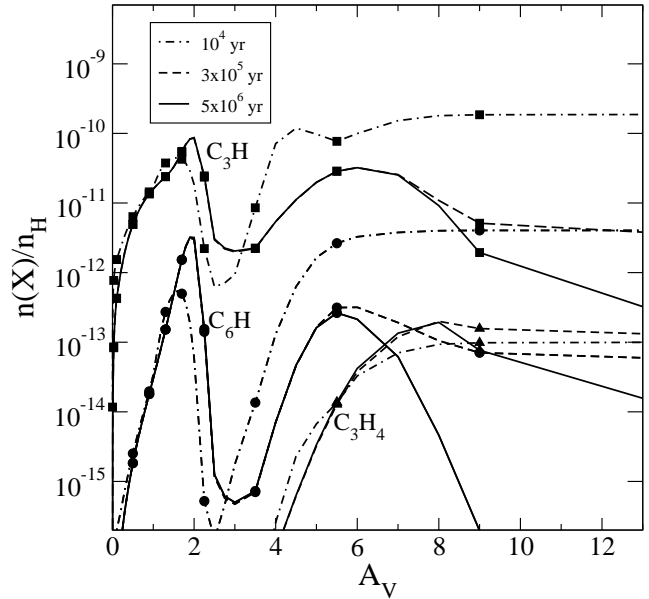


Figure 3. Same as Fig. 2, but for the molecules C_3H (filled squares), C_6H (filled circles), and C_3H_4 (filled triangles).

which contains 419 species and 4103 reactions. This relatively old version of the `osu` network was used for a variety of reasons. First, it was the model with which the original calculations were begun. During the calculations, several newer versions of the network (`osu.2005`) were prepared, but required modifications and corrections, which were not fully resolved until the summer of 2007. To determine if the newest version of the `osu` code (`osu.03.2008`; see <http://www.physics.ohio-state.edu/~eric/>) leads to any significant changes, we have run a new version of our standard model with this network. The differences are discussed in Appendix A.

We assume that our dense PDR is formed as a result of the process of star formation inside a dense cloud, when radiation from a new star begins to affect the chemistry of the surrounding gas. Thus, we assume that, at $t = 0$, the gas has already undergone chemical evolution during $\sim 10^5$ yr under dense conditions: a density $n_{\text{H}} = 2 \times 10^4 \text{ cm}^{-3}$ and $T = 10 \text{ K}$. The initial abundances are those of a typical dark cloud (see Table 1) as derived from the values measured for smaller species (composed of up to five atoms) in TMC-1CP (Smith et al. 2004). For those smaller species where there is no available observed value, we adopted the fractional abundances calculated by Smith et al. (2004) at 10^5 yr. In our model, we maintain the standard depleted cosmic abundance ratios $\text{C}/\text{H} = 7.3 \times 10^{-5}$ and $\text{O}/\text{H} = 1.76 \times 10^{-4}$. Since the total C/H abundance measured in TMC-1P is a factor ~ 2 less than the standard cosmic ratio, we have assumed that the remaining C is locked up in CO , with the initial abundance shown in Table 1. The initial abundance of atomic O is then chosen so that the overall standard depleted O/H abundance is used. We discuss in Section 4.3 other possible results using the lower initial abundances of CO .

The $t = 0$ values listed in Table 1 are more general than those found for TMC-1, where a much more complex

Table 2. Peak fractional abundances and A_V for selected hydrocarbons in the standard model

Species	$t = 10^4$ yr		$t = 3 \times 10^5$ yr		$t = 5 \times 10^6$ yr	
	$n(X)/n_H$	A_V	$n(X)/n_H$	A_V	$n(X)/n_H$	A_V
CH ₄	5.5×10^{-9}	7.0	2.3×10^{-8}	8.0	2.4×10^{-8}	8.0
CH	1.6×10^{-8}	1.1	1.9×10^{-8}	1.6	1.9×10^{-8}	1.6
C ₂ H	9.3×10^{-9}	1.0	1.2×10^{-8}	1.6	1.2×10^{-8}	1.6
CH ₂	1.4×10^{-8}	1.1	7.3×10^{-9}	1.8	7.3×10^{-9}	1.8
C ₂ H ₂	4.2×10^{-9}	13.0	1.5×10^{-9}	8.0	1.5×10^{-9}	8.0
CH ₃	2.3×10^{-10}	2.0	2.4×10^{-10}	2.2	2.4×10^{-10}	2.2
C ₄ H	8.7×10^{-11}	13.0	9.2×10^{-11}	1.8	9.5×10^{-11}	1.8
C ₃ H	1.9×10^{-10}	13.0	8.6×10^{-11}	2.0	8.7×10^{-11}	2.0
C ₃ H ₂	1.0×10^{-9}	13.0	6.2×10^{-11}	1.9	6.3×10^{-11}	1.9
C ₅ H	1.0×10^{-11}	13.0	9.6×10^{-12}	1.9	9.9×10^{-12}	2.0
C ₂ H ₃	5.6×10^{-12}	1.7	8.0×10^{-12}	2.0	8.0×10^{-12}	2.0
C ₆ H	4.0×10^{-12}	13.0	3.1×10^{-12}	1.9	3.2×10^{-12}	1.9
C ₂ H ₄	4.0×10^{-13}	13.0	1.8×10^{-12}	9.0	1.9×10^{-12}	8.0
C ₄ H ₂	2.5×10^{-10}	13.0	2.1×10^{-12}	8.0	1.8×10^{-12}	7.0
C ₈ H	2.0×10^{-13}	9.0	2.7×10^{-13}	2.0	2.7×10^{-13}	2.0
C ₃ H ₄	1.0×10^{-13}	13.0	2.0×10^{-13}	8.0	1.9×10^{-13}	8.0
C ₃ H ₃	1.3×10^{-14}	13.0	3.3×10^{-14}	7.0	5.8×10^{-14}	7.0
C ₅ H ₂	5.2×10^{-12}	13.0	3.2×10^{-14}	7.0	3.5×10^{-14}	7.0
C ₇ H	4.4×10^{-13}	13.0	4.6×10^{-14}	6.0	2.7×10^{-14}	5.5
C ₄ H ₃	1.3×10^{-13}	13.0	2.3×10^{-14}	7.0	2.5×10^{-14}	7.0
CH ₃ C ₄ H	1.1×10^{-13}	13.0	2.1×10^{-14}	7.0	2.2×10^{-14}	7.0
C ₆ H ₂	5.4×10^{-12}	13.0	2.1×10^{-14}	13.0	1.6×10^{-14}	7.0
C ₆ H ₆	4.7×10^{-14}	13.0	1.2×10^{-14}	7.0	2.1×10^{-15}	7.0

molecule development has already occurred, which appears to be unique.

3 RESULTS

Fig. 1 shows the fractional abundance profiles of H, H₂, C, C⁺, and CO obtained with our standard model at selected times up to steady state (5×10^6 yr). Such a profile at $t = 0$ would be totally flat at the value given in Table 1. Here the three layers described in Sect. 2 can be distinguished. The crossing point between the fractional abundances of H and H₂ moves inwards with time, and it is found at $A_V \sim 0.04$ at steady-state. The low value for this visual extinction is somewhat artificial; proper inclusion of factors such as a lower density and higher temperature at the cloud edge and a less efficient surface formation of H₂ would increase the extinction at crossing. Further into the cloud, CO becomes the most abundant carbon-bearing species at $A_V \sim 1.7$, while C becomes more abundant than C⁺ at visual extinctions between 3 and 8.5.

3.1 Hydrocarbons

Figs 2 and 3 show the fractional abundances of several hydrocarbon molecules as a function of A_V for our standard model at three different times: $t = 10^4$, 3×10^5 , and 5×10^6 yr. The first two times correspond, respectively, to an early time in the evolution when only the outermost layers are approaching steady state, and a time when steady-state is virtually reached in the outer to intermediate regions of the PDR ($A_V < 3 - 5$). In addition to the figures, Table 2 shows

the peak fractional abundances and corresponding visual extinctions of most hydrocarbons present in our model at the three different times. In this and subsequent tables of fractional abundances, the order of presentation is in terms of decreasing steady-state peak fractional abundance.

The evolution of the fractional abundances of a hydrocarbon depends upon whether the molecule is present initially in the gas, a group that includes C₂H, C₄H, and C₃H₂, or whether it is not, a group that includes both complex species and hydrogenated species such as CH₄ and C₃H₄. As emphasized in Fig. 4, the main difference is that the molecules pertaining to the first group (C₂H in Fig. 4) go through an early phase of selective destruction before reaching steady-state, while the molecules belonging to the second group (CH₄ in Fig. 4) start with a phase of formation.

Looked at in more detail, the unsaturated hydrocarbons initially present in the gas are quickly heavily destroyed in the very outer layers of the PDR, while the destruction is much slower in more shielded layers. By a time of a few $\times 10^4$ yr, fractional abundance peaks are found at $A_V \sim 1.5 - 2$ with a value close to that of steady-state. As time progresses, steady-state is reached for the outer parts, while the fractional abundances in the inner layers may drop several orders of magnitude before steady-state is reached at $t \sim 5 - 10 \times 10^6$ yr. The end result is a large decrease in abundance from the initial value for the outermost layers ($A_V < 1$) and a significant decrease, very much dependent on the molecule, for slabs with $A_V > 7$.

The molecules that were not present initially in the gas (e.g. CH₄, CH₂) initially show a larger increase in the deeper layers of the cloud. We usually find the highest abundance for each A_V at a time $t \sim 10^4$ yr or shortly thereafter. After

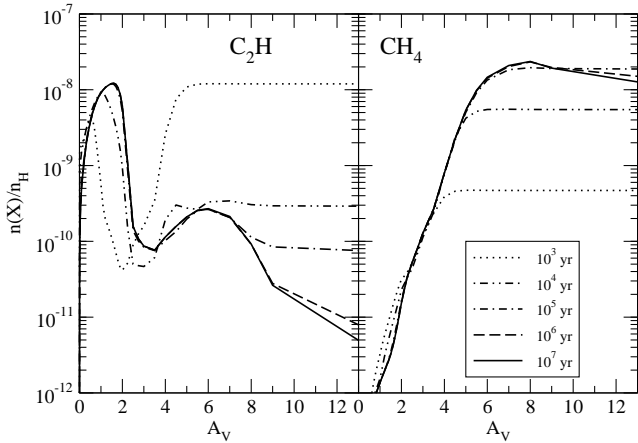


Figure 4. Fractional abundances with respect to n_{H} for the molecules C_2H (left panel) and CH_4 (right panel) as a function of A_V in our standard model for five different times: 10^3 , 10^4 , 10^5 , 10^6 , and 10^7 yr. The solid lines represent steady-state abundances.

this moment, the evolution of the fractional abundances of these molecules is similar to the one described for the previous group: the fractional abundances do not change appreciably in the outer parts of the PDR ($A_V \sim 1-2$) while the abundances may drop, although not so dramatically, in the inner layers until reaching steady-state conditions at $t \sim 5-10 \times 10^6$ yr. Interestingly, CH_4 abundance does not follow this description completely for $A_V > 3$, where it keeps increasing until a time $\sim 5 \times 10^4$ yr. Then, it shows very little variation, and it only decreases very slightly for $A_V > 8$.

All hydrocarbons show a similar abundance profile at steady state (or even at earlier times): their fractional abundances grow with depth into the cloud until they reach a peak, after which the fractional abundance decreases with depth more or less drastically. The peak position and the steepness of the decrease depend on the hydrocarbon. As can be seen in Table 2, the more unsaturated and simpler hydrocarbons typically peak in outer layers of the cloud, while as the number of C atoms grows or as the molecules become more hydrogenated, the peaks are found deeper into the cloud. For instance, by steady state, C_2H peaks at $A_V = 1.6$; C_3H_2 , at $A_V = 1.9$; C_8H , at $A_V = 2.0$; and CH_4 , at $A_V = 8$. This distribution is not continuous; there seem to be two main regions, $A_V = 1.5-2$ and $A_V = 5.5-8$, where all the peaks are found. In fact, most of the hydrocarbons show two peaks at those two ranges, the relative importance of which seems to depend on the number of carbon atoms present or on being or not saturated. This secondary peak (primary in some cases) is due to the bump in C abundance shown in Figure 1. Hydrocarbons containing fewer carbon atoms typically reach larger fractional abundances; for example, CH_4 , C_2H and C_4H are some of the most abundant hydrocarbons.

3.2 HCN, HNC, and cyanopolyynes

Fig. 5 shows the evolution of the fractional abundance profiles for the HCN and HNC molecules, and the cyanopolyynes HC_3N , HC_5N , HC_7N , and HC_9N , while Table 3 lists the abundance peaks and the A_V where they are

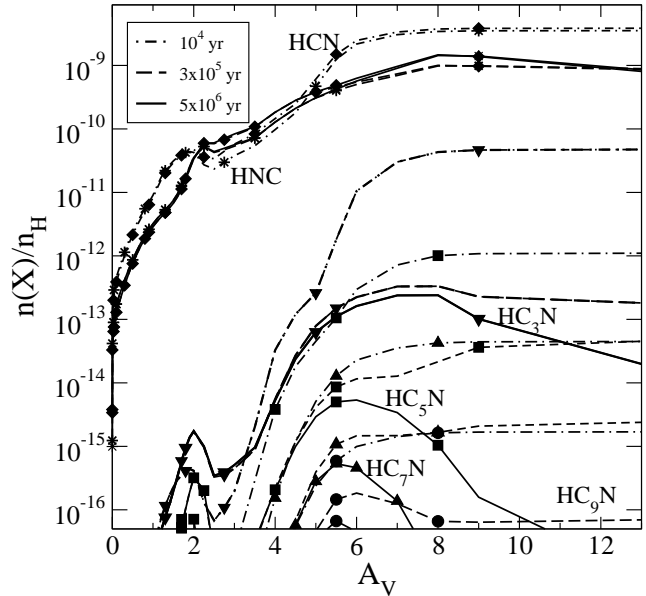


Figure 5. As Fig. 2, but for the molecules HCN (diamonds), HNC (stars), HC_3N (filled triangles pointing down), HC_5N (filled squares), HC_7N (filled triangles pointing up), and HC_9N (filled circles).

found. Initially present in the gas, HC_3N experiences a progressive diminution in all the slabs as time progresses, which is particularly severe in the first 10^5 yr. When steady-state is reached, HC_3N shows a profile with two peaks, a very low one at $A_V \sim 2$, and the main one at $A_V \sim 8$. Unlike the case for hydrocarbons, the abundance of HC_3N in the deepest layers is less than an order of magnitude below that at the peak.

The more complex cyanopolyynes show a behaviour similar to those unsaturated hydrocarbons not present initially in the gas. First, they go through a phase of formation until they achieve maximum abundances at all A_V at a time $t \sim 10^4$ yr, when peak abundances are in the inner regions. Then they are progressively destroyed at all optical depths. The steady-state profiles of these molecules show a low abundance peak at $A_V \sim 2$, the main abundance peak, one or two orders of magnitude over the secondary peak, at $A_V \sim 4-8$, and a decrease at deeper layers.

The initially-present HCN and HNC molecules show a completely different but nearly identical behaviour (see Table 3). Their destruction is very intense in the first 10^4 yr for slabs $A_V < 2$, while only moderate for the deeper layers. The destruction goes on until a time $t \sim 10^5$ yr, when there is a slight increase of abundances for $A_V \sim 3-8$, before steady-state is reached. An abundance peak then exists at $A_V = 5.5$ and a slightly lower, but almost uniform, abundance occurs at deeper layers. As happened with the cyanopolyynes, there is a small bump in abundance at $A_V \sim 2.1$, approximately 20 times lower than the main peak.

3.3 Other molecules

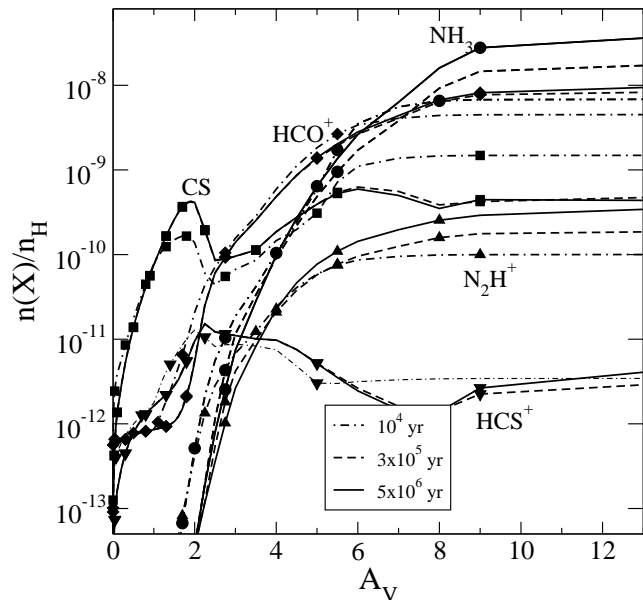
Fig. 6 shows the abundance profiles at assorted times of CS , HCO^+ , NH_3 , and N_2H^+ , all of which are well-known species in dense regions. The peak abundances at the selected times

Table 3. Peak fractional abundances and A_V for cyanopolyynes, HCN, and HNC

Species	$t = 10^4$ yr		$t = 3 \times 10^5$ yr		$t = 5 \times 10^6$ yr	
	$n(X)/n_H$	A_V	$n(X)/n_H$	A_V	$n(X)/n_H$	A_V
HCN	3.9×10^{-9}	13.0	1.0×10^{-9}	8.0	1.5×10^{-9}	8.0
HNC	3.5×10^{-9}	13.0	9.9×10^{-10}	9.0	1.4×10^{-9}	8.0
HC ₃ N	4.7×10^{-11}	13.0	3.3×10^{-13}	8.0	2.4×10^{-13}	8.0
HC ₅ N	1.1×10^{-12}	13.0	4.5×10^{-14}	13.0	5.4×10^{-15}	6.0
HC ₇ N	4.5×10^{-14}	13.0	2.4×10^{-15}	13.0	5.3×10^{-16}	5.5
HC ₉ N	1.7×10^{-15}	13.0	1.8×10^{-16}	6.0	6.7×10^{-17}	5.5

Table 4. Peak fractional abundances and A_V for other molecules typically detected in dense clouds

Species	$t = 10^4$ yr		$t = 3 \times 10^5$ yr		$t = 5 \times 10^6$ yr	
	$n(X)/n_H$	A_V	$n(X)/n_H$	A_V	$n(X)/n_H$	A_V
NH ₃	6.8×10^{-9}	13.0	1.7×10^{-8}	13.0	3.6×10^{-8}	13.0
HCO ⁺	4.5×10^{-9}	13.0	8.3×10^{-9}	13.0	9.4×10^{-9}	13.0
H ₂ CO	1.2×10^{-9}	13.0	1.1×10^{-9}	7.0	1.1×10^{-9}	7.0
CS	1.5×10^{-9}	13.0	6.3×10^{-10}	6.0	5.9×10^{-10}	6.0
N ₂ H ⁺	1.0×10^{-10}	13.0	1.9×10^{-10}	13.0	3.4×10^{-10}	13.0
HCS ⁺	1.3×10^{-11}	2.0	1.5×10^{-11}	2.2	1.5×10^{-11}	2.2

**Figure 6.** As Fig. 2, but for the molecules CS (filled squares), HCO⁺ (filled diamonds), NH₃ (filled circles), N₂H⁺ (filled triangles pointing up), and HCS⁺ (filled triangles pointing down).

are listed in Table 4. Present in the initial gas, CS shows a fractional abundance profile quite similar to unsaturated hydrocarbons with two peaks of very similar abundances, the inner one ~ 1.5 times larger than the outer one, but with a very small fall in abundance for the deeper layers, where abundance is very close to constant.

The species HCO⁺, NH₃, and N₂H⁺ show profiles some-

what similar to those of HCN and HNC. Unlike these latter two species, however, the fractional abundance peak of the three molecules is found in the innermost slab of our model.

One common thread running through these descriptions of assorted profiles is the following: the dominant features of the fractional abundance profiles as a function of A_V for most species show a strong similarity to plots of the fractional abundance of the same molecules as a function of time in homogeneous dark cloud models (see e.g., Taylor, Morata & Williams 1998). The so-called ‘early-time’ molecules, such as CS or C₂H, peak in the outer layers of the PDR, while the ‘late-time’ molecules, such as NH₃, N₂H⁺, or HCO⁺, peak in the innermost layers. This is not too surprising; the early-time chemistry in the homogeneous cloud (based on a high abundance of atomic C) is similar to that in the PDR layers with $A_V \sim 1-2$, while the late-time chemistry (based on a high abundance of CO) is similar to that in the inner layers.

4 INFLUENCE OF PHYSICAL PARAMETERS

4.1 Radiation field

In order to determine how the external radiation field affects the abundances of the different species, especially the hydrocarbons, we ran three additional models, each with a different intensity of the radiation field, indicated by scaling factors of $\chi = 10$, 10^3 , and 10^4 . Fig. 7 compares the results of our standard model with the results obtained with a model using $\chi = 10^4$ at an early stage of evolution, 10^4 yr, and at 10^7 yr, when steady-state has been reached for all A_V . Table 5 lists the peak abundances of a variety of species for three times when $\chi = 10^4$.

Table 5. Peak fractional abundances and A_V for selected molecules for a model with $\chi = 10^4$

Species	$t = 10^4$ yr		$t = 3 \times 10^5$ yr		$t = 1 \times 10^7$ yr	
	$n(X)/n_H$	A_V	$n(X)/n_H$	A_V	$n(X)/n_H$	A_V
CH ₄	5.7×10^{-9}	9.0	2.3×10^{-8}	13.0	2.3×10^{-8}	13.0
NH ₃	6.7×10^{-9}	13.0	1.1×10^{-8}	13.0	1.9×10^{-8}	13.0
CH	6.0×10^{-9}	2.5	1.2×10^{-8}	3.0	1.2×10^{-8}	3.2
HCO ⁺	4.4×10^{-9}	13.0	6.8×10^{-9}	13.0	7.1×10^{-9}	13.0
CH ₂	4.6×10^{-9}	2.5	5.4×10^{-9}	3.2	5.5×10^{-9}	3.2
C ₂ H	8.1×10^{-10}	2.5	3.3×10^{-9}	3.0	3.3×10^{-9}	3.2
C ₂ H ₂	4.1×10^{-9}	13.0	1.7×10^{-9}	13.0	1.6×10^{-9}	13.0
HCN	3.8×10^{-9}	13.0	1.1×10^{-9}	13.0	1.6×10^{-9}	13.0
HNC	3.5×10^{-9}	13.0	1.0×10^{-9}	13.0	1.5×10^{-9}	13.0
H ₂ CO	1.2×10^{-9}	13.0	1.1×10^{-9}	9.0	1.1×10^{-9}	9.0
CS	1.5×10^{-9}	13.0	9.0×10^{-10}	9.0	8.7×10^{-10}	9.0
N ₂ H ⁺	9.9×10^{-11}	13.0	1.6×10^{-10}	13.0	2.6×10^{-10}	13.0
CH ₃	9.2×10^{-11}	7.0	1.2×10^{-10}	6.0	1.2×10^{-10}	6.0
C ₃ H ₂	1.0×10^{-9}	13.0	7.1×10^{-11}	9.0	7.3×10^{-11}	9.0
C ₃ H	1.9×10^{-10}	13.0	5.5×10^{-11}	9.0	5.6×10^{-11}	9.0
C ₄ H	8.7×10^{-11}	13.0	1.6×10^{-11}	9.0	1.6×10^{-11}	9.0
C ₂ H ₄	3.9×10^{-13}	13.0	2.1×10^{-12}	13.0	2.4×10^{-12}	13.0
C ₂ H ₃	1.4×10^{-12}	7.0	2.2×10^{-12}	8.0	2.2×10^{-12}	8.0
C ₄ H ₂	2.3×10^{-10}	13.0	2.5×10^{-12}	13.0	1.9×10^{-12}	13.0
C ₅ H	1.0×10^{-11}	13.0	8.3×10^{-13}	9.0	7.6×10^{-13}	9.0
C ₆ H	4.1×10^{-12}	13.0	7.9×10^{-13}	9.0	7.0×10^{-13}	9.0
HC ₃ N	4.5×10^{-11}	13.0	3.4×10^{-13}	13.0	2.5×10^{-13}	13.0
C ₃ H ₄	9.8×10^{-14}	13.0	2.3×10^{-13}	13.0	2.0×10^{-13}	13.0
C ₈ H	2.0×10^{-13}	13.0	1.3×10^{-13}	9.0	1.1×10^{-13}	9.0
C ₇ H	4.4×10^{-13}	13.0	1.1×10^{-13}	9.0	8.5×10^{-14}	9.0
C ₃ H ₃	1.3×10^{-14}	13.0	3.4×10^{-14}	9.0	4.4×10^{-14}	9.0
C ₅ H ₂	5.1×10^{-12}	13.0	2.9×10^{-14}	13.0	2.8×10^{-14}	9.0
C ₄ H ₃	1.3×10^{-13}	13.0	2.1×10^{-14}	9.0	2.3×10^{-14}	9.0
CH ₃ C ₄ H	1.1×10^{-13}	13.0	1.9×10^{-14}	13.0	1.4×10^{-14}	9.0
HC ₅ N	1.1×10^{-12}	13.0	2.6×10^{-14}	13.0	1.3×10^{-14}	9.0
C ₆ H ₂	5.3×10^{-12}	13.0	1.9×10^{-14}	13.0	1.2×10^{-14}	9.0
C ₆ H ₆	4.7×10^{-14}	13.0	1.1×10^{-14}	9.0	3.2×10^{-15}	9.0

The evolution of the fractional abundances when $\chi = 10^4$ differs most strongly from the standard case, as the right-hand side of Fig. 7 shows, in the sweeping of most of the molecular species from the outer layers by the intense radiation. Most of the molecules shown have already disappeared from the layers with $A_V < 1$ by $t = 10^4$ yr and, when steady-state is reached at 10^7 yr, there are no significant molecular abundances at slabs with $A_V < 1$. Even molecular hydrogen disappears from the external layers as the position at which H₂ becomes the most abundant form of hydrogen increases to $A_V \sim 1.3$ when $\chi = 10^4$. Thus, for the model with $\chi = 10^4$, the gas at $A_V < 1$ is mostly in atomic form. The fractional abundance peaks of the species with profiles that peak in the outer layers are consequently found deeper into the cloud at all times, the typical effect being an increase from $A_V \sim 1.5$ –2 to $A_V \sim 3$ –4 (and the inner maxima and/or enhancements from $A_V \sim 4.5$ –7 to $A_V \sim 7$ –9). On the other hand, the results for the model with a less intense radiation field than the standard model, $\chi = 10$, are the opposite and many molecular species have significant fractional abundances at A_V as low as 0.1. The fractional abundance peaks are then located in more external layers of the cloud.

The maximum fractional abundances are also modified by the intensity of the radiation field in all of the cases. As χ is increased from 100 to 10^4 , the outer peak abundance of hydrocarbons is typically reduced by a factor of $\lesssim 10$, but the decrease can range from very little, as for CH₂, to two (C₄H or C₆H) or three (C₈H) orders of magnitude. On the other hand, the ‘inner’ abundance peak of hydrocarbons increases by a small factor, between 2 and 10, and in some cases, such as C₃H₂, it can become larger than the (outer) peak abundance in the standard model.

The peak fractional abundances of the cyanopolyynes have a much greater dependence on the radiation field, and we find general enhancements of two and three orders of magnitude for the outer layers, when $\chi = 10^4$. This increase does not change the fact that there are only traces of these molecules in these layers. The peak abundance at high visual extinction also increases with a larger radiation field, but only by small factors (2–3).

The radiation field is able to modify the chemistry even in deep slabs of the cloud. We find that even if the changes in intermediate layers ($A_V \sim 5$ –8) can be small, a factor of a few, they are non-zero; only the gas at $A_V \gtrsim 9$ –10 is completely shielded from the radiation for all the models

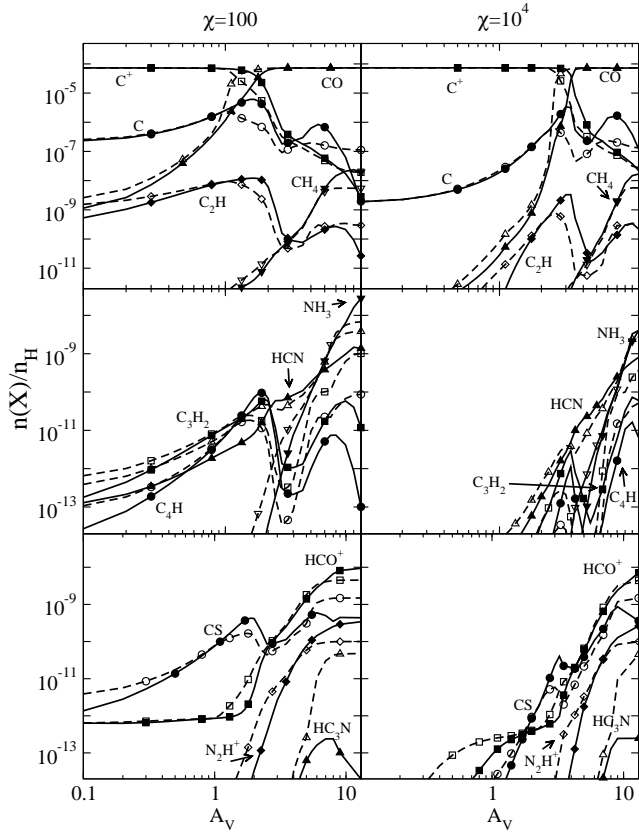


Figure 7. Comparison of the fractional abundances obtained with (left-hand panel) the standard model and (right-hand panel) with a model using $\chi = 10^4$. The results are shown at an early time, 10^4 yr (dashed lines and open symbols), and at 10^7 yr (solid lines and filled symbols), when steady-state has been reached.

and does not show any significant changes at any time between the different models. As a result, for the two radiation fields considered, all the molecules that reach their maximum abundances in the inner cloud, such as HCN, NH_3 , and N_2H^+ , have approximately the same abundances at high visual extinction at steady-state and at intermediate times. On the other hand, these same molecules, which were not abundant in the outer layers of the cloud for $\chi = 100$, completely disappear from the superficial layers for $\chi = 10^4$.

4.2 Density and temperature

In order to explore the effects of different densities and temperatures, we reran our standard model, modifying either the density or the temperature of the gas. The densities and temperatures used were $n_{\text{H}} = 10^3, 10^5$, and 10^6 cm^{-3} , and $T = 10, 100$, and 200 K .

The effects of density change bear some similarities with the effects of the radiation field: a higher density increases the shielding and the abundances of most of the molecules in the outer layers of the cloud; a lower density on the other hand, clears these same layers of much molecular material, and displaces the peak abundance position to deeper parts of the cloud. The results are not identical, particularly in the way the inner and outer peaks of many molecules change with density.

Table 6. Atomic initial abundances

Element	$n(\text{X})/n_{\text{H}}$
H	1
He	0.14
C^+	7.3×10^{-5}
N	2.14×10^{-5}
O	1.76×10^{-4}
S^+	8×10^{-8}
Si^+	8×10^{-9}
Fe^+	3×10^{-9}
Na^+	2×10^{-9}
Mg^+	7×10^{-9}
P^+	3×10^{-9}
Cl^+	4×10^{-9}

Unsaturated hydrocarbons (C_2H , C_4H , C_6H , C_8H) show an increase in the peak abundance in the outer abundance peak with increasing density, that can range from a few percent (C_2H) to an order of magnitude (C_4H , C_6H); and a simultaneous decrease in the abundance of the inner abundance peak, which can be almost three orders of magnitude for the molecules containing more than a few carbon atoms. The resulting effect is that at high densities there is only a narrow range of A_V in the outer layers of the cloud where these molecules show a significant abundance; the more carbon atoms they contain, the narrower the range. At the lowest density, on the other hand, the inner abundance peak may not only be larger than the outer abundance peak, but also larger than the peak abundance in the standard model. Hydrocarbons that peak inside the cloud, such as methane and C_3H_4 , also show a clear increase in abundance as density increases. At $n = 10^6 \text{ cm}^{-3}$, methane also shows an outer peak.

The rest of the molecules we have discussed in Section 3 also show clear trends in peak abundance with a change in density. The cyanopolyynes show a steep increase in the abundance in the outer layers as density increases (it can reach three or more orders of magnitude), but never exceed the inner peak abundance, which does not change much and is found at slightly lower A_V . At the higher density, HC_3N reaches 10^{-12} cm^{-3} for times $\sim 5 \times 10^5$ yr. The abundance of the radical CS increases slightly with density (up to a factor of 4 in the outer parts of the cloud), whereas HCO^+ shows a behaviour similar to the unsaturated hydrocarbons, but with changes typically less than an order of magnitude: the peak abundance at high density is a factor ~ 8 lower than for the standard model. NH_3 and N_2H^+ show similar trends as HCO^+ , but while the fractional abundance decrease at $n = 10^6 \text{ cm}^{-3}$ is less than a factor of 3 for NH_3 , it is larger than 30 for N_2H^+ .

Variations in the peak fractional abundance with temperature as we raise T to 200 K tend to be less dramatic than with density. The differences in fractional abundance in the outer layers relative to our standard model are rarely larger than a factor of 2, and often show less than a 50 per cent change. The differences are larger for the inner layers, where a few molecules show a change of more than an order of magnitude for $T = 200 \text{ K}$. Most of the carbon chains (except C_2H or C_6H) show a large decrease of abundance (~ 100) in the innermost layers as T increases, whereas for

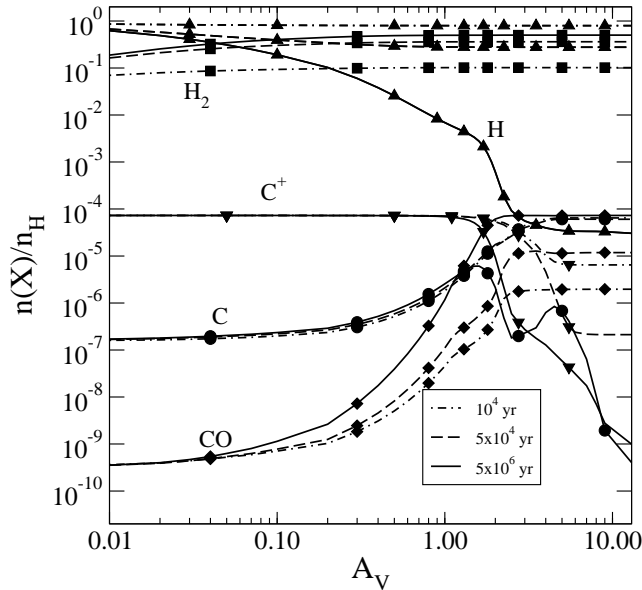


Figure 8. As Fig. 1 for a model with atomic initial abundances.

the outer layers only C_2H , C_6H , and C_8H show an increase in abundance with temperature. The fractional abundances of CH_4 , H_2CO , CS , and the cyanopolynes HC_3N and HC_5N also diminish with increasing T , while the abundances of HCN and HNC increase in the outer layers with T (a factor of ~ 3 at $T = 200$ K), but decrease in the inner layers (less than 40 per cent). The ions HCO^+ and N_2H^+ show increasing abundance with increasing temperature (a factor of ~ 2 for $T = 200$ K). The abundances of the rest of the molecules that we discussed in Section 3 show small changes of a few percent.

4.3 Initial abundances

The previous models were all run assuming as initial abundances those expected if a dense PDR is created by a star recently formed inside a molecular cloud. In order to explore the dependence of the model on the initial fractional abundances, it is also interesting to determine what are the differences between our standard model and other models that have different initial fractional abundances.

First, we compare our standard model with a model starting from gas that is atomic in nature. Figures 8 and 9 show some results obtained with a model identical to our standard model, but using the initial abundances listed in Table 6, derived from ‘low metal’ abundances (Ruffle & Herbst 2000). The major difference between Fig. 8 and its analogous, Fig. 1, is that, with standard initial abundances, H_2 decreases at low A_V as a function of time whereas, with atomic initial abundances, H_2 must be synthesized and increases at all A_V as a function of time. Fig. 9 clearly shows that the different initial abundances determine the early evolution of the gas. The first years are obviously spent in the process of building more complex molecules from the available elements, while, in our standard model, a general destruction of initially present molecules is predominant for very early times. Table 7 lists the maximum abundances and peak positions of several interesting species

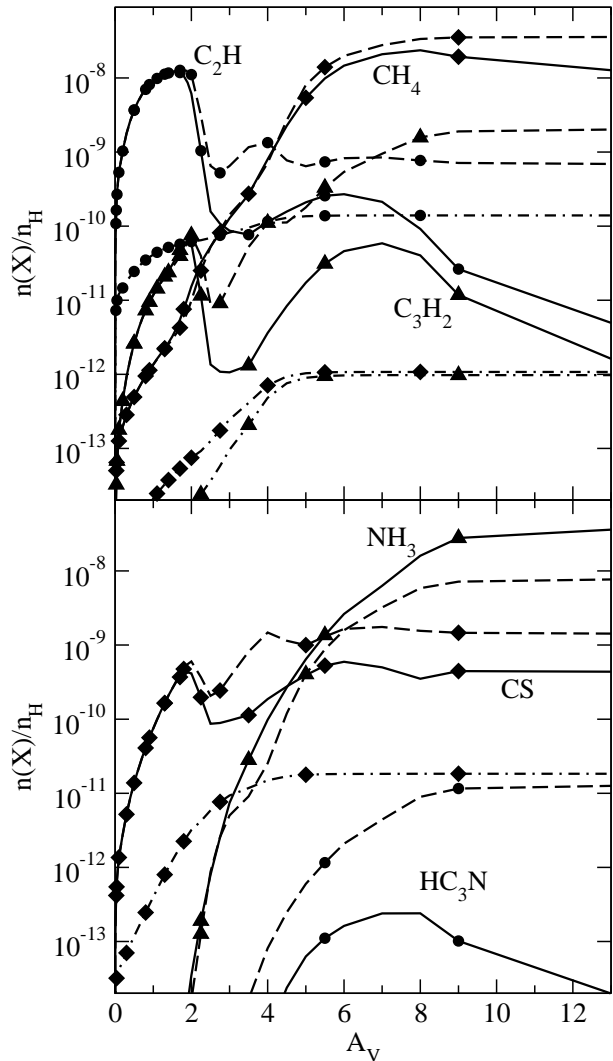


Figure 9. Fractional abundance profiles for a model with atomic initial abundances and $\chi = 100$ at three times: 10^4 yr (dot-dashed lines), 3×10^5 yr (dashed-lines) and 5×10^6 yr (solid lines). Some hydrocarbons are shown on the top figure; viz., C_2H (filled circles), C_3H_2 (filled triangles up), and CH_4 (filled diamonds). On the bottom figure are depicted HC_3N (filled circles), NH_3 (filled triangles up), and CS (filled diamonds).

at selected times. Much lower than in the standard model for a time $t = 10^4$ yr, the fractional abundances show an increase as A_V grows until a plateau is reached. By $1-3 \times 10^5$ yr, the fractional abundances of some molecules, such as many carbon chains and cyanopolynes, can be much larger at $A_V > 3$ than for the standard model at the same times, from factors of 2-3 to more than ~ 1000 . Eventually, after a few $\times 10^5$ yr when most of the C begins to be locked in the CO molecule, the abundances for many molecules in the inner layers follow the same evolutionary path as in the standard model and start decreasing, while there is still a slight increase in the molecular abundances in the outer layers. The net effect is a change from the ‘plateau’ profile to the same peaked profiles we observe for most species in our standard model. Interestingly, the abundances of HCO^+ , NH_3 , and N_2H^+ , which peak in the innermost layers, are smaller than

Table 7. Peak fractional abundances and A_V for selected molecules for a model with atomic initial abundances and $\chi = 100$

Species	$t = 10^4$ yr		$t = 3 \times 10^5$ yr		$t = 5 \times 10^6$ yr	
	$n(X)/n_H$	A_V	$n(X)/n_H$	A_V	$n(X)/n_H$	A_V
NH ₃	4.0×10^{-15}	13.0	7.7×10^{-9}	13.0	3.6×10^{-8}	13.0
CH ₄	1.1×10^{-12}	13.0	3.6×10^{-8}	13.0	2.4×10^{-8}	8.0
CH	1.8×10^{-10}	1.1	1.9×10^{-8}	1.8	1.9×10^{-8}	1.7
C ₂ H	1.4×10^{-10}	13.0	1.3×10^{-8}	1.8	1.2×10^{-8}	1.6
HCO ⁺	7.3×10^{-12}	13.0	6.7×10^{-9}	13.0	9.4×10^{-9}	13.0
CH ₂	3.7×10^{-12}	1.0	6.4×10^{-9}	1.7	7.3×10^{-9}	1.8
C ₂ H ₂	5.2×10^{-12}	13.0	1.1×10^{-8}	13.0	1.5×10^{-9}	8.0
HCN	9.2×10^{-13}	13.0	9.6×10^{-10}	13.0	1.5×10^{-9}	8.0
HNC	7.4×10^{-13}	13.0	9.0×10^{-10}	13.0	1.4×10^{-9}	8.0
H ₂ CO	1.5×10^{-12}	13.0	1.2×10^{-9}	7.0	1.1×10^{-9}	7.0
CS	1.8×10^{-11}	13.0	1.8×10^{-9}	7.0	5.9×10^{-10}	6.0
N ₂ H ⁺	1.9×10^{-15}	7.0	1.2×10^{-10}	13.0	3.4×10^{-10}	13.0
CH ₃	4.9×10^{-12}	7.0	2.7×10^{-10}	3.5	2.4×10^{-10}	2.2
C ₄ H	3.7×10^{-11}	13.0	5.0×10^{-10}	7.0	9.6×10^{-11}	1.8
C ₃ H	1.2×10^{-12}	13.0	5.7×10^{-10}	9.0	8.7×10^{-11}	2.0
C ₃ H ₂	9.8×10^{-13}	13.0	2.0×10^{-9}	13.0	6.3×10^{-11}	1.9
C ₅ H	1.6×10^{-12}	13.0	2.7×10^{-10}	6.0	9.9×10^{-12}	2.0
C ₂ H ₃	3.8×10^{-17}	0.9	7.0×10^{-12}	2.2	8.0×10^{-12}	2.0
C ₆ H	3.3×10^{-13}	13.0	3.4×10^{-10}	6.0	3.2×10^{-12}	1.9
C ₂ H ₄	9.7×10^{-20}	13.0	5.4×10^{-12}	13.0	1.9×10^{-12}	8.0
C ₄ H ₂	6.9×10^{-12}	13.0	1.4×10^{-9}	13.0	1.8×10^{-12}	7.0
C ₈ H	6.9×10^{-15}	13.0	1.5×10^{-10}	5.0	2.7×10^{-13}	2.0
HC ₃ N	1.1×10^{-17}	13.0	1.3×10^{-11}	13.0	2.4×10^{-13}	8.0
C ₃ H ₄	9.2×10^{-21}	13.0	6.4×10^{-12}	13.0	1.9×10^{-13}	8.0
HC ₅ N	6.0×10^{-17}	13.0	3.0×10^{-11}	13.0	5.4×10^{-15}	6.0
C ₆ H ₆	5.0×10^{-20}	13.0	3.6×10^{-12}	13.0	2.1×10^{-15}	7.0

the ones in the standard model for times $t < 1 - 2 \times 10^6$ yrs. Steady state is reached at $t \sim 10^7$ yr at all A_V . The abundances at steady state are the same or almost identical (< 1 per cent) to the fractional abundances of the standard model.

As we pointed out in Section 2, the CO initial fractional abundance of our standard model is greater than the one measured in TMC-1P by a factor ~ 2 . In order to see how this can affect our conclusions, we ran two additional models that used the CO abundance listed by Smith et al. (2004) for TMC-1: i) a model (Model CO-1) maintaining the total standard elemental amount of C and O, and ii) a model (Model CO-2) not maintaining either the C/H ratio of 7.3×10^{-5} or the O/H ratio of $= 1.76 \times 10^{-4}$. Table 8 shows the initial abundances of C, O, and CO for these models, as well as the overall C/H, O/H, and C/O elemental abundance ratios, designated with the subscript ‘*elem*’. As an example, Fig. 10 shows the C₂H abundances in these two models relative to the C₂H abundance in our standard model.

For the first model, the more abundant initial free C in the gas produces a smaller abundance of CO for times $\lesssim 2 \times 10^5$ yrs and a correspondingly larger abundance of C and C⁺ up to $3-5 \times 10^5$ yrs. This effect is particularly important for atomic C in the inner layers. For early times, the free carbon produces an increase of the abundance of all the carbon-chain molecules, at all layers $A_V \gtrsim 2$. These differences in abundance relative to the standard model diminish with time from the outer to the inner layers, and last up to $5-10 \times 10^5$ yrs for layers $A_V \gtrsim 3 - 4$. The differences

Table 8. Initial abundances of C, O, and CO [$n(X)/n_H$] for various models

species	Standard Model	Model CO-1	Model CO-2
CO	7.27×10^{-5}	4.00×10^{-5}	4.00×10^{-5}
C	2.81×10^{-8}	3.27×10^{-5}	2.81×10^{-8}
O	1.03×10^{-4}	1.36×10^{-4}	1.03×10^{-4}
(C/H) _{elem}	7.27×10^{-5}	7.27×10^{-5}	4.00×10^{-5}
(O/H) _{elem}	1.76×10^{-4}	1.76×10^{-4}	1.43×10^{-4}
(C/O) _{elem}	0.41	0.41	0.28

in abundance at the positions of the external peak abundances of the standard model are generally very small. For early times, the abundances at layers with $2 \lesssim A_V \lesssim 5$ can be significantly larger by factors between a few (for CH₄) and up to $10^3 - 10^4$ (for C₆H), while for layers with $A_V \gtrsim 5$, most of the carbon-chain molecules show abundances that range from ~ 25 to a few hundred times larger than the ones in the standard model at early times. Other carbon-containing molecules show a similar behaviour. On the other hand, HCO⁺ and NH₃ show smaller abundances, by factors of 3–4, for layers $A_V < 6$. For times later than $\sim 10^6$ yr, the abundances are practically identical to the ones from the standard model, as we expected from the results of the model with initial atomic abundances.

Although the late-time abundances for the second

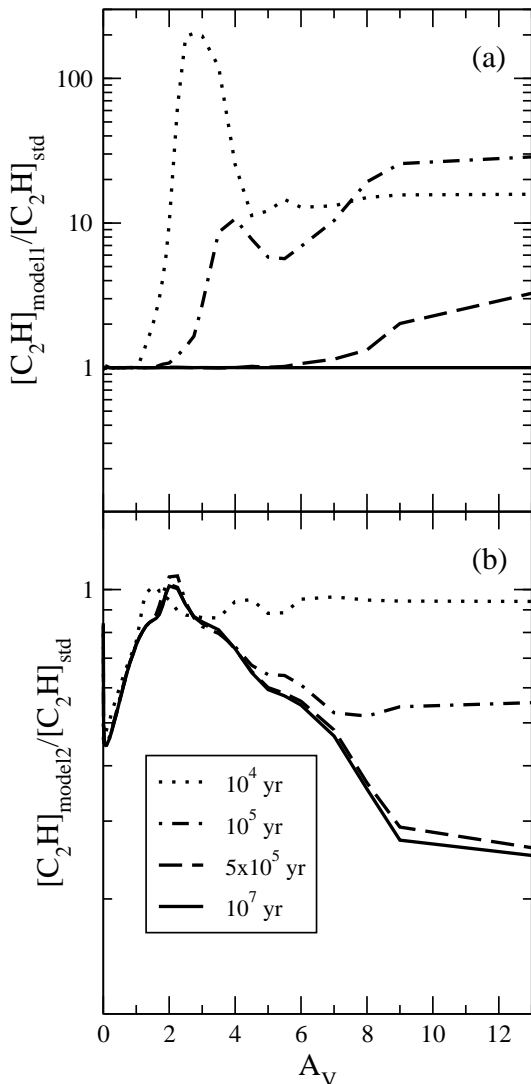


Figure 10. (a) (upper panel) C_2H abundance in Model CO-1 compared with our standard model as a function of A_V at four times: 10^4 yr (dotted lines), 10^5 yr (dot-dashed lines), 5×10^5 yr (dashed-lines) and 10^7 yr (solid lines); (b) (lower panel) as in a) but for Model CO-2.

model are relatively close, generally less than an order of magnitude, to those of our standard model, the early- and late-time behaviour of most of the species is opposite to that of the first model, i.e. an even closer agreement to our standard model is found at early times. At later times, the lower general abundance of elemental C produces smaller abundances compared to the standard model for all the carbon-chain molecules. This effect is specially apparent in the inner layers, $A_v > 3$, with factors that range from 2 to more than 10. Also at later times, the differences in the outer layers are usually less than 50 per cent, and in some cases we can see a slight increase in abundance, as is the case for C_3H_2 or C_6H , but never affecting the abundance peaks of the standard model. This slight increase can also be seen for HNC, HC_3N , and HCO^+ . The abundance of NH_3 is larger by factors of 1.5–4 at all layers.

5 COMPARISON WITH OBSERVATIONS OF THE HORSEHEAD NEBULA

One of the main difficulties in the modelling of PDRs is to compare the results with actual observations, because it is usually extremely difficult to determine the distribution of the gas density, and the way the far-UV radiation penetrates the cloud. In recent times, the Horsehead nebula has been used as a benchmark for PDR models, because it appears to be viewed edge-on and thus offers a good opportunity to study the structure of a PDR.

The Horsehead nebula (B33) is located at the western edge of the molecular cloud L1630, at the near side of the H II region IC 434. The Horsehead is thought to be an early Bok globule; i.e., a higher density cloud core which is emerging from its parental and more tenuous cloud as the UV radiation from the O9.5V star σ Ori further to the west erodes the surrounding gas (Reipurth & Bouchet 1984). The Horsehead nebula has been extensively studied at many different wavelengths, from the early maps in CS, CO, and [C II] (Lada, Bally & Stark 1991; Zhou et al. 1993; Kramer, Stutzki & Winnewisser 1996) to more recent observations ranging from the mid-IR to the millimetre (Abergel et al. 2002, 2003; Pound, Reipurth & Bally 2003; Teyssier et al. 2004; Habart et al. 2005; Pety et al. 2005). The gas density derived from these observations, either from the excitation of molecular lines or from the penetration depth of the UV radiation, is $1\text{--}4 \times 10^4 \text{ cm}^{-3}$ (Zhou et al. 1993; Kramer et al. 1996; Abergel et al. 2003). Habart et al. (2005) found that the gas density follows a steep gradient at the cloud edge, rising to $n_H = 10^5 \text{ cm}^{-3}$ in less than 0.02 pc, and at the same time the gas temperature changes from $\sim 200\text{--}300$ K to $\sim 10\text{--}20$ K. Abergel et al. (2003) derived a kinetic temperature from single-dish observations of 30–40 K, which would correspond to the bulk of the cloud, while the warm UV-illuminated edge would have higher temperatures (Pety et al. 2005). The far-UV incident radiation field can be considered to have a mild intensity, $\chi \sim 60$ in Draine units, and has also been estimated in the $\chi \sim 20\text{--}200$ range (Zhou et al. 1993; Kramer et al. 1996; Abergel et al. 2003).

Teyssier et al. (2004) and Pety et al. (2005) studied the physical and chemical structure of B33 at millimetre wavelengths, using moderate-angular-resolution single-dish and high-angular-resolution interferometric observations, respectively. Teyssier et al. (2004) observed the emission of a variety of molecules ($C^{18}O$, C_2H , C_3H , C_4H , C_3H_2 , C_3H_4 , C_6H , $HN^{13}C$, HC_3N , and CS) at three positions in the Horsehead nebula, one coinciding with the peak in IR emission (IR peak), another, very close by, at the position at the hydrocarbon peak emission, and the last one at the position of the CO peak. These and previous observations showed a relative stratification of H_2 and small hydrocarbons: the boundary of the H_2 emission corresponds to the edge of the PDR, while the hydrocarbon peaks, which are well correlated with one another, are located farther into the cloud. In addition, the CO peak occurs at a place tangential to the hydrocarbon peak. Teyssier et al. (2004) used steady-state PDR models with the same physical conditions as ours to explain the original observations, with reaction rates from two different networks, UMIST95 (Millar, Farquhar & Willacy 1997) and osu.2003 (Smith et al. 2004). They reproduced some of the observed fractional abundances ($C^{18}O$ and C_2H) and some

column density ratios, but their calculated peak fractional abundances for $c\text{-C}_3\text{H}_2$ and C_4H are low by an order of magnitude. The discrepancies were attributed to the return of small carbon molecules to the gas phase through the sputtering of small carbon grains and PAHs.

The high-angular-resolution observations of Pety et al. (2005) determined the column density and fractional abundance of C^{18}O , C_2H , C_4H , and $c\text{-C}_3\text{H}_2$ at three positions, named ‘IR edge’, ‘IR peak’, and ‘cloud’, in order of their depth inside the cloud. The ‘IR-edge’ position corresponds to the edge of the PDR, where the UV radiation is most intense; the ‘IR peak’ position is located 5 arcsec east, where both the IR and hydrocarbon emission peaks of Teyssier et al. (2004) were found; and the ‘cloud’ position is ~ 15 arcsec deeper into the cloud. The gas temperature estimates for the three positions are 100, 60, and 40 K. Pety et al. (2005) also used different models to try to fit the more spatially detailed observations but the main results are not significantly different from the ones of Teyssier et al. (2004). Recently, Pety et al. (2007) published more data for CS , HCS^+ , and HCO^+ at three positions, one approximately at the ‘cloud’ position and two deeper into the molecular cloud.

The results of our standard model when steady-state is reached are generally similar to those of Teyssier et al. (2004) and Pety et al. (2005) (with either reaction network) concerning the details of the PDR zones and the positions and heights of the hydrocarbon peaks. We compare in Figs 11 and 12 the abundance profiles of our standard model at three different times with the fractional abundances of some molecules observed by Pety et al. (2005) and Teyssier et al. (2004), taking into account the errors associated with the observations. In these figures, fractional abundance is plotted against visual extinction, determined from position for the observational values by assuming a constant density of $2 \times 10^4 \text{ cm}^{-3}$. The peaking of fractional abundances towards the outer layers of the PDR in both observation and theory is striking.

Let us first consider the results at steady-state (5×10^6 yr), focusing initially on the molecules studied at high resolution by Pety et al. (2005). The peak fractional abundances of C_2H , C_4H , and C_3H_2 in our standard model are similar to those of the model of Teyssier et al. (2004). Compared with observation (see Fig. 11), we find reasonably good agreement at all three observational positions for C_2H (less so for the ‘cloud’ position, although a slight displacement of $\Delta A_V \sim 0.25$ would fit the three points at the same time). For C_4H and C_3H_2 , the value observed at the ‘cloud’ position is the only one matched by our model, within a factor of 2 for C_4H . The underproduction for the other two positions is $\sim 10^2 - 10^3$ times for C_4H and $\lesssim 50$ times for C_3H_2 .

Fig. 12 show the additional species detected by Teyssier et al. (2004) and Pety et al. (2007) compared to the results of our standard model. We note that their so-called IR peak and hydrocarbon peak positions are assumed to both be represented by visual extinctions from 0 to 2. To convert the actual observation of HN^{13}C and H^{13}CO^+ into the normal isotopologue, we assumed a $^{12}\text{C}/^{13}\text{C}$ ratio of 62 (Langer & Penzias 1993). As can be seen, the steady-state results of our standard model range from good to poor. CS and HCS^+ are reproduced within a factor of ~ 3 , which for the first could probably be attributed to the effects of sulfur

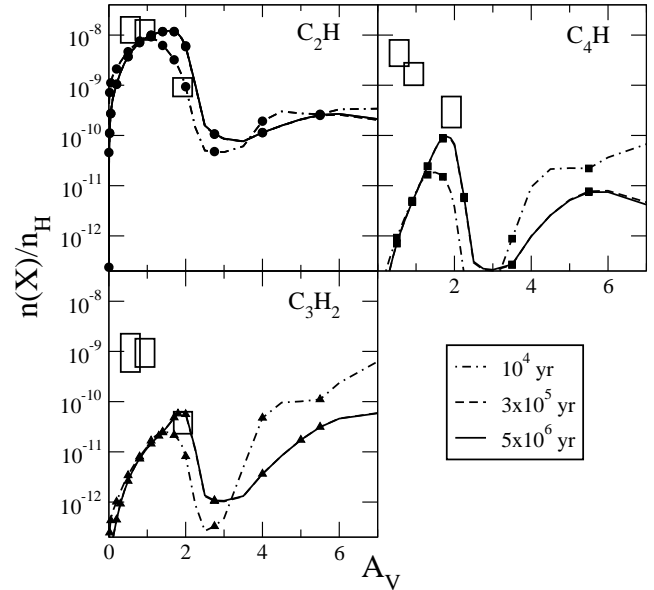


Figure 11. Comparison of the abundance profiles of our standard model for C_2H , C_4H , and C_3H_2 at three times with the values observed by Pety et al. (2005) at the three positions, labelled from left to right as ‘IR-edge’, ‘IR-peak’, and ‘cloud’. The boxes indicate the uncertainties in the observed fractional abundances and in the position (beamwidth).

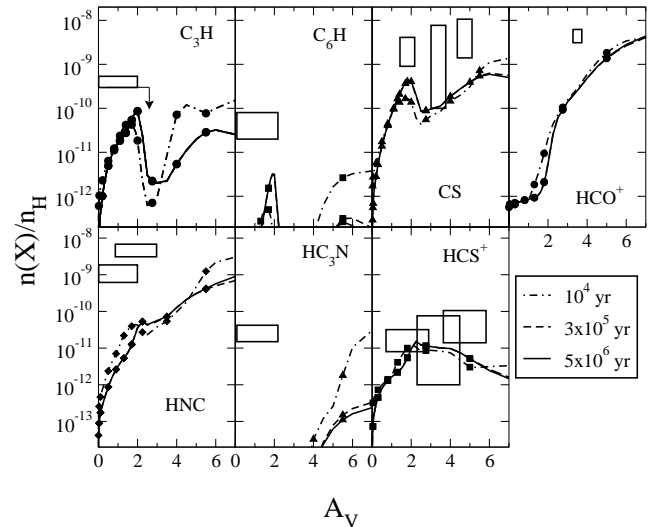


Figure 12. Similar to Fig. 11, but for C_3H , C_6H , HNC , and HC_3N in the ‘IR peak’ or ‘hydrocarbon peak’ positions observed by Teyssier et al. (2004) and for CS , HCO^+ , and HCS^+ taken from Pety et al. (2007).

depletion. C_3H and C_6H are underproduced in the model, similarly to the other carbon chains, by factors of ~ 3 and ~ 6 , respectively. The abundances of HCO^+ and HNC are almost a factor of 10 below the observed value, although there are values in the model at high A_V that match the observations. We find the largest differences for HC_3N , which is heavily underproduced in the standard model at steady state.

If we consider earlier times, we find that for times of 10^4 yr and later, most of the time dependence occurs in

inner portions of the PDR, such as the ‘cloud’ position of Pety et al. (2005) and even larger values of visual extinction. For the ‘cloud’ position, we find that the abundance profiles of C_2H may be somewhat better fitted at earlier times. In general, the results of Teyssier et al. (2004) do not extend far enough into the cloud to be sensitive to time. There is a large time dependence for the abundance of HC_3N but this occurs at high values of visual extinction for the most part. Since variations in the CO initial abundances discussed in Sect. 4.3 mainly affect abundances in inner layers, with little or no impact on the outer peak abundances, these variations do not greatly affect the level of agreement between model and observation.

5.1 Other physical parameters

We used the alternative models discussed in Sect. 4 to determine if there is a set of physical parameters that agrees better than the standard model with the abundances derived from the observations in the Horsehead nebula. We also ran additional models that looked at intermediate values of the parameters or that changed initial conditions. We did not find a unique best-fit model. Since different authors (e.g., Pety et al. 2005; Goicoechea et al. 2007) have proposed different elemental abundances to try to explain the abundances in PDRs, we have also changed the relative elemental abundance, mainly by increasing the abundance of C, but also of O, S, and N. An initial carbon abundance twice of that in our standard model shows some of the better agreements for C_4H (for the innermost position), C_6H , and especially CS and HCS^+ . ‘Carbon-rich’ abundances similar to the ones used by Millar et al. (2000) overproduce the abundances of most of the carbon-containing molecules. Different sulfur abundances can be used to fine tune the amounts of CS and HCS^+ . We also explored the effects of different values of the cosmic ray ionization rates. We used values of 0.5, 10, 50, and 100 times the standard value of ζ . Typically, higher values of the cosmic-ray photodissociation rate ($\geq 10 - 50$) show better agreements for many of the observed molecules, especially combined with a slightly higher density and temperature and/or slightly less intense radiation field.

5.2 Age of the PDR

The time dependence of our models, as is also the case for the time-dependent model of UCL (Bell et al. 2005), can in principle be used to try to set an age for a dense PDR, given a favourable geometry. For the Horsehead nebula, Pound et al. (2003) argue that, from its size and velocity gradient, the formation time scale could be as short as a few $\times 10^5$ yr, and the object is likely to be destroyed in 5×10^6 yr. These time scales are shorter or comparable to the time needed by our standard model to reach steady-state. But, in trying to distinguish between steady-state and earlier times by chemical abundance profiles, we must keep in mind some formidable obstacles. First, the uncertainties in the determination of the PDR geometry and density structure make such an analysis very difficult because they obscure purely temporal effects. Secondly, there is a dependence of early-time results on what is chosen for initial abundances.

Thirdly, the abundance profiles of the many hydrocarbons that peak in the outer layers of the cloud show greater sensitivity to time in the inner layers of the PDR because steady-state takes more than 10 times longer to reach in the inner slabs. Unless the PDR is very young, these inner slab abundances are likely to be much smaller than peak values and thus hard to observe. Moreover, most of the more abundant molecules that peak in the deep slabs of the cloud also reach values close to those of steady-state in a relatively short time and may not help much in the determination of age. Some molecules, such as HC_3N , suffer large variations in fractional abundance in the same span of time and in the position of the peak abundance, and these could be useful to carry out age estimates. In some of the models we ran, we find better agreements for some molecules at times $0.4 - 3 \times 10^5$ yrs, but given the uncertainties in the observations and in the density structure of the cloud, we need more observations of different positions and molecular transitions to have a clearer view of the structure of the PDR and to be able to make a more precise estimate of its age. In particular, we would need observations of the layers with $A_V \gtrsim 4$, where we find, in our model, the largest variations of abundance for most of the observed molecules.

6 SUMMARY

We present the results of a time-dependent model of a dense photon-dominated region created after a star has formed inside a dark cloud. We have assumed for our standard model an homogeneous cloud with density $n = 2 \times 10^4$ cm^{-3} and gas temperature $T = 40$ K, on one side of which impinges an FUV radiation field $\chi = 100$ times the ISRF.

We have found that the more unsaturated and/or simpler hydrocarbons, in particular C_2H , C_4H , or C_6H , have peak fractional abundances in the outer layers of the PDR, at $A_V \sim 1-2$, at times as early as a few $\times 10^4$ yr, while more saturated hydrocarbons, such as CH_4 , have their peaks deeper into the cloud at these times, around $A_V \sim 5$. The outer and intermediate layers reach steady-state rapidly, at times shorter than a few $\times 10^5$ yr, while for the inner layers it takes almost an order of magnitude longer.

The molecule CS and the cyanopolynes also peak nearer to the surface of the cloud, at $A_V \sim 1.7-2$, at times following a few $\times 10^4$ yr, while HCN, HNC, HCO^+ , N_2H^+ and NH_3 peak deeper into the clouds, from $A_V = 5.5$ onwards. This result is very interesting because it reproduces in space a similar distribution of molecules to the one found in time for a homogeneous gas-phase model. The external radiation field seems to keep the chemistry ‘young’ in the outer layers of the cloud, while only the more shielded slabs develop a ‘late-time’ chemistry.

We have run several models with modifications of some of the parameters of the standard model, varying the intensity of the radiation field, the temperature and density of the cloud, and the initial distribution of fractional abundances in the gas. For the three models run with non-standard scaling factors of the radiation field of 10, 10^3 , and 10^4 , the effects on the peak fractional abundances of hydrocarbons are not large, typically about an order-of-magnitude. At large values of the radiation field, all molecules are swept out of the outer regions, while only the gas at $A_V > 9 - 10$ is

completely shielded from variations in the radiation field. One salient result of increasing the density is that for hydrocarbons that peak in the outer layers, the abundance profile when plotted against distance has a smaller region of large fractional abundance. Another salient feature is that the peak fractional abundances of selected hydrocarbons and cyanopolyynes increase with density in the range $10^3 - 10^6 \text{ cm}^{-3}$ while other species show little change or even a decrease. Variations in peak fractional abundance as temperature is changed tend to be less significant than with density for temperatures in the range 10-200 K. We also explored the effects that different initial fractional abundances have on the results of the model by running a model that starts with atoms in the gas, finding that the evolution of fractional abundances in time is very different from the standard model, although the end result (steady state) is, of course, the same.

In a comparison of the results of our standard model with recent high-angular resolution observations of the Horsehead nebula, we were able to reproduce, within the estimated observational uncertainties, the peak fractional abundance and spatial dependence of C_2H ; not so with C_4H and C_3H_2 which show much worse agreements at the outermost positions. For the rest of the molecules, studied at moderate- and high-angular resolution, the agreement to the observations go from good (for CS and HCS^+) to poor (especially for HC_3N). We have also used additional models to explore how different physical conditions can improve the agreement with observations. Even if some models did reproduce better some of the molecular abundances, we could not find a single model that was able to fit all the observations at the same time.

We also ran two models in which the initial CO abundance was changed from its 'standard' value of 7.3×10^{-5} with respect to total H. First, we reduced this value to that measured in TMC1-CP (4×10^{-5}), while conserving the total elemental abundances of C and O by increasing the atomic abundances of carbon and oxygen. Secondly, we used the reduced CO abundance with no attempt to maintain our standard elemental abundances of C and O. In both instances, little change was seen for carbon-chain species from the standard model at times near steady state. At earlier times, however, the first modification produces strong enhancements in carbon-chain molecules for the inner layers while the second modification produces smaller diminutions of these abundances that are even smaller than at steady state. The status of the agreement with observations in the Horsehead nebula is unaffected by changes in the initial CO abundance, since the changes affect the inner layers, which have not been observed.

Recently, there have been some new results that might help to solve the disagreement between observation and theory. First, Rimmer and Herbst (in preparation) have recalculated the cosmic-ray ionization rate as a function of depth into clouds. We found in our models that a different value of ζ may dramatically change the abundances of the species. Secondly, there is evidence that calculations including negative ions may indeed increase the calculated abundances of neutral carbon chain species. These calculations are currently being done by R. Ni Chiumin, Tom Millar, Nanase Harada, Eric Herbst and others. Thirdly, Roueff et al. (2007) have confirmed that the Horsehead

Nebula is rather clumpy by their analysis of deuterated molecules. We intend to use these new calculations in further work to find out if they are able to reproduce the abundances of the molecules observed in the Horsehead nebula.

From the currently available observational data, it is difficult to obtain a definitive age of the Horsehead nebula. We would need more observations, especially of layers deep into the cloud ($A_V \gtrsim 4$), where the abundances of species such as hydrocarbons and cyanopolyynes are more sensitive to changes in time.

7 ACKNOWLEDGEMENTS

E. H. wishes to thank the National Science Foundation (U. S.) for support of his research programme in astrochemistry. OM acknowledges the support of the National Science Foundation to the astrochemistry group at Ohio State University.

REFERENCES

- Abergel A., Bernard J. P., Boulanger F., Cesarsky D., Falgarone E., Jones A., Miville-Deschenes M.-A., Perault M., Puget J.-L., Hultgren M., et al. 2002, *A&A*, 389, 239
- Abergel A., Teyssier D., Bernard J. P., Boulanger F., Coulais A., Fossé D., Falgarone E., Gerin M., Perault M., Puget J.-L., et al. 2003, *A&A*, 410, 577
- Bell T. A., Viti S., Williams D. A., Crawford I. A., Price R. J., 2005, *MNRAS*, 357, 961
- Draine B. T., 1978, *ApJSS*, 36, 595
- Draine B. T., Bertoldi B., 1996, *ApJ*, 468, 269
- Fuente A., Rodríguez-Franco A., García-Burillo S., Martín-Pintado J., Black J. H., 2003, *A&A*, 406, 899
- Goicoechea J. R., Pety J., Gerin M., Teyssier D., Roueff E., Hily-Blant P., 2007, *arXiv:astro-ph/0703393*
- Habart E., Abergel A., Walmsley C. M., Teyssier D., Pety J., 2005, *A&A*, 437, 177
- Hollenbach D. J., Tielens A. G. G. M., 1997, *ARA&A*, 35, 179
- Kramer C., Stutzki J., Winnewisser G., 1996, *A&A*, 307, 915
- Lada E. A., Bally J., Stark A. A., 1991, *ApJ*, 368, 432
- Langer W. D., Penzias A. A., 1993, *ApJ*, 408, 539
- Le Petit F., Roueff E., Le Boulrot J., 2002, *A&A*, 390, 369
- Lee H.-H., Herbst E., Pineau des Fôrets G., Roueff E., Le Boulrot J., 1996, *A&A*, 311, 690
- Millar T. J., Farquhar P. R. A., Willacy K., 1997, *A&AS*, 121, 139
- Millar T. J., Herbst E., Bettens, R. P. A., 2000, *MNRAS*, 316, 195
- Pety J., Goicoechea J. R., Gerin M., Hily-Blant P., Teyssier D., Roueff E., Habart E., Abergel A., 2007, in Lemaire S. L., Combes, F., eds, *Molecules in Space and Laboratory*. S. Diana, p. 13
- Pety J., Teyssier D., Fossé D., Gerin M., Roueff E., Abergel A., Habart E., Cernicharo J., 2005, *A&A*, 435, 885
- Pound W., Reipurth B., Bally J., 2003, *AJ*, 125, 2108
- Reipurth B., Bouchet P., 1984, *A&A*, 137, L1
- Roueff E., Parise B., Herbst E., 2007, *A&A*, 464, 245
- Ruffle D. P., Herbst E., 2000, *MNRAS*, 319, 837

- Smith I. W. M., Herbst E., Chang Q., 2004, MNRAS, 350, 323
 Taylor S. D., Morata O., Williams D. A., 1998, A&A, 336, 309
 Teyssier D., Fossé D., Gerin M., Pety J., Abergel A., Roueff A., 2004, A&A, 417, 135
 Wagenblast R., Hartquist T. W., 1989, MNRAS, 237, 1019
 Zhou S., Jaffe D. T., Howe J. E., Geis N., Herrmann F., Madden S. C., Poglitsch A., Stacey G. J., 1993, ApJ, 419, 190

APPENDIX A: CALCULATIONS MADE WITH THE NEWEST RATEFILE OSU_03_2008

The calculations discussed in the body of the paper were performed with the `osu.2003` network for a variety of reasons. We have also used the latest version of this network without molecular carbon chain anions (`osu_03_2008`) to determine if there are any substantial changes in the standard version of our model. Some salient differences found are as follows:

(i) The abundance of molecular hydrogen is unchanged, and there is very little change in the abundance of atomic hydrogen ($\sim +3$ per cent at $A_V \sim 2$, ~ -3 per cent in the innermost layers). The crossing of the H and H₂ abundances is at $A_V \sim 0.04$. CO abundances are ~ -5 per cent up to $A_V \sim 2$, while C shows the opposite behaviour. Abundances of C⁺ at layers $A_V > 4$ are a factor of ~ 25 per cent less.

(ii) Differences between abundances are quite small for most molecules (from a few percent to a factor of 2) at steady state, especially for the more abundant hydrocarbons, for which they are typically much less than a factor of two, except at middle layers ($A_V \sim 4-7$), where these differences can go from 25 per cent less for C₂H to a factor of 2 less for C₃H₂. The main apparent effect is a slightly lower inner abundance peak for some of these molecules. Other neutrals show very small differences, such as HCN (abundances 20 per cent larger or lower overall, except a factor of 2 less at $A_V \sim 4$) or H₂CO (with almost no changes, less than 5 per cent). HCO⁺ shows up and down variations of about 20 per cent at steady state. Some less abundant hydrocarbons and other low abundance species may show larger differences at some positions but always at positions where they have very low abundance.

(iii) N₂H⁺ is generally larger with the newer network, with differences up to a factor of five at some outer layers at steady state, where the ion is less abundant. At the inner layers, the differences range from 50 per cent to 20 per cent from early times to steady state. Ammonia does not show this behavior; its abundance is at most ~ 70 per cent larger at middle layers at steady state, but small differences, less than 10 per cent in the rest between the two networks at steady state (differences of ~ 40 per cent at early times).

(iv) CS and HCS⁺ have lower abundances with the newer network, with maximum differences a factor of 3-5 for CS and 2-15 for HCS⁺, especially for the outer layers, and for $t > 5 \times 10^4$ yr. At the same time, SO and SO₂ show larger abundances for layers $A_V > 6$, of ~ 70 per cent and a factor of about 4, respectively, at steady state (with smaller differences at earlier times).

(v) HC₃N has a larger abundance at steady state, by almost an order of magnitude, for the outer layers, where it is less abundant, and of ~ 2 in the inner layers. At earlier times, the abundances at the inner layers can be a factor of ~ 5 larger. The other cyanopolyynes tend to have slightly lower abundances overall, except a drop at $A_V \sim 5$ that can be about an order of magnitude, but they have very low abundances in both cases.

(vi) In comparison with the observational results for the Horsehead Nebula, there are few significant differences. CS and HCS⁺ would be the most affected molecules, specially the latter. Nonetheless, the HCS⁺ abundances at $A_V \sim 2-4$ would still be inside the error bars of the abundance determined by the observations.